A Procedure for the Automated Detection of Magnetic Field Inversion in SOHO MDI Magnetograms

S.S. Ipson, V.V.Zharkova, S.I. Zharkov and A. Benkhalil

Department of Cybernetics, University of Bradford, BD7 1DP, UK
s.s.ipson@bradford.ac.uk

Abstract. Magnetic inversion lines are generally constructed from line-of-sight magnetic field data which have been smoothed to reduce the resolution scale of the data. This eliminates the fine details of the magnetic inversion lines found in regions of strong magnetic field. The paper presents a new approach to constructing magnetic neutral lines, based on a distance transform, which aims to construct neutral lines retaining fine detail in regions of strong magnetic field while reducing the detail elsewhere. The method of implementation is described and results obtained are compared with those obtained by applying Gaussian smoothing to solar magnetograms and with filaments visible in an Hα image for 2002 July.

1 Introduction

Solar phenomena such as sunspots, filaments, flares and active regions vary with an 11 (22) year cycle, which means they are connected with the behaviour of the solar magnetic field [1], [2]. The solar magnetic field measured with the line-of-sight (LOS) ground-based or space-based magnetographs ([3], [4]), or recent full vector magnetographs ([5], [6]) provides an important data resource for understanding and predicting solar activity. The importance of magnetic field has been emphasized in many theoretical works including: heating of the solar atmosphere; formation and support of multi-levelled magnetic loops and filaments resting on top of them; activation of energy releases in solar flares and coronal mass ejections; and in many other small and large scale events occurring in the solar atmosphere and interplanetary space. It is thought that different scales of magnetic field magnitudes account for solar events of different scales and that event scenarios result mostly from magnetic configurations of loops with opposite magnetic polarities. For example, solar filaments often appear on the boundaries of coronal holes ([7], [8] , [9]) or above a middle line between two-ribbon flares ([10], [11]) that usually is very close to the location of magnetic inversion lines, or magnetic neutral lines (MNLs).

This paper is concerned with the construction of magnetic neutral lines from line-of-sight magnetograms and four different approaches have been identified in the literature. In the vicinity of active regions contour methods have been used. An example of this approach is the work of Falconer *et al*. [12], investigating neutral-line magnetic shear and enhanced coronal heating in solar active regions. They defined

the MNL to be the region between the -25 G and +25 G contours. In the regions of interest MNLs were found to be 2 pixels wide or less. However, away from active regions, the regions between the -25 G and +25 G contours become very wide. Several authors have presented methods for identifying magnetic field boundaries between large regions of predominantly positive or negative polarity. For example, Bornmann *et al*. [13], used morphological operators to extend the strongest positive and negative regions which were then added to the original magnetograms and smoothed. Two thresholds were used to identify the limits to the neutral line locations. Durrant [14] remapped magnetograms to a latitude-longitude grid applied smoothing over circles of diameters 60, 120 and 180 arc seconds and then transformed back to the original geometry. Smoothed magnetograms were displayed using 256 shades of grey with positive magnetic fields using the upper half of the range with increasing field magnitude displayed with increasing darkness and negative magnetic fields use the lower half of the grey range with increasing field magnitude corresponding to increasing darkness. The zero-field contour is marked by the discontinuity in the greyscale between mid-grey and peak white. Ulrich *et al* [15], reported a method of averaging magnetogram data over multiple observations at different times, after taking differential rotation at different latitudes into account, and extracting the east-west and meridional components of the slowly evolving large-scale magnetic field to get improved magnetic and neutral line synoptic maps.

This paper presents an approach to determining magnetic neutral lines which aims to retain the local detail of MNLs in regions of high field while simultaneously constructing boundaries between larger scale positive and negative magnetic regions.

2 Method

Solar magnetograms are produced by a number of the ground and space based observatories. However, this paper is concerned with magnetograms produced by the Michelson Doppler Instrument (MDI) installed on the SOHO spacecraft. The magnetograms produced by this instrument provide an array of 1024 by 1024 pixel measurements of the line of sight component (the dominant component of the magnetic vector field in the central portion of the disk) of the solar magnetic field in the photosphere. The radius of the solar disc in these magnetograms is about 489 pixel (corresponding to a pixel resolution of about 2 arc sec) and the magnetograms are produced at a rate of one per minute except during periods of occasional down-time. The magnetogram pixel values are stored using16 bits, with a signal range from about -1500 G to +1500 G and a noise level of about ±20 G.

Several studies, (e.g. [16], [17], and [18]) have shown that the general magnetic field of the sun consists of small (1-2 arc sec) but intense (~ 1200 G) flux knots of mixed polarity. In some regions the flux knots are fairly evenly distributed while in others one polarity dominates and at low resolution observation masks those of the other polarity to give what is often described as a unipolar region. In a typical example of an MDI magnetogram from SOHO the boundary between adjacent positive and negative magnetic regions is well defined only at comparatively few locations between local concentrations of opposite field associated with sun spots. Elsewhere,

positive (and negative) regions are indicated by the presence of mainly positive (or negative) fluctuations from the ±20 G, near zero, range of magnetic field intensity defined by the noise level. The boundaries between positive and negative regions of an MDI magnetogram generally have a great deal of fine structure, as is hinted at by the magnetograms shown at the top left corner in Figs. 1 and 2 which have the minimum smoothing in the two sets of magnetograms. This fine detail can be reduced by local averaging of individual magnetograms (e.g. [14]) or by averaging, after differential rotation, all available magnetograms for a Carrington rotation (e.g. [15]). This paper examines another approach which is applied to a single magnetogram and is capable of retaining the structure of neutral line boundaries in high field regions, while reducing the fine detail elsewhere.

The principal idea for the automatic construction of boundary lines separating adjacent collections of small positive magnetic features from adjacent collections of small negative magnetic features is to grow the features isotropically (using a distance transform) and to mark the points where the positive and negative regions make contact. The resulting points are used as estimates of points along inversion lines. The initial seed regions are obtained by applying positive and negative thresholds of equal magnitude which defines the solar disk into three regions: positive regions, negative regions and neutral regions within which the neutral lines are found. The specific steps used to construct the inversions lines in this illustration are as follows.

The magnetogram data are first read from the fits file and stored in a floating point array. The data is then segmented into the three types of magnetic regions by applying a two level magnetic field threshold ± T, where T could be set at the noise level 20 G say. A fast Euclidean distance transform, based on the approach of Cuisenaire and Macq [19], is applied to determine the distances of the pixels in the neutral region from the nearest segmented boundary pixel. This is implemented as indicated in the following pseudo code. First three array buffers, x, y and z, with dimensions the same as the magnetogram are initialised. The elements of x, y and z, store the horizontal and vertical spatial offsets and the distances from the nearest object respectively. The array elements with positions corresponding to the positive and negative regions defined by the threshold are initialised to zero and the remaining elements are set to values larger than any which will be encountered during the computation.

A first pass is made through the data, from left to right and bottom to top, updating the buffer elements in sequence. During this pass, at the end of each row a reverse scan is made of each row, updating the buffers.

```
Initialise buffers x[N, N], y[N, N] and z[N, N]
Set row index I = 1
    Set column index J = 1
        If current position has x[J, I] or y[J, I] greater than 0
            If J > 1 Compute dx = x[J-1, I] + 1, dy = y[J-1, I], d = dx^2 + dy^2
                If d < z[J, I]
                        z[J, I] = d, x[J, I] = dx, y[J, I] = dy
            if I > 1 Compute dx = x[J, I-1], dy = y[J, I-1] + 1, d = dx^2 + dy^2
                If d < z[J, I]
                        z[J, I] = d, x[J, I] = dx, y[J, I] = dy
```

```
    Increment J and, if J <= N, repeat
    Set column index J = N-1
        If current position has x[J, I] or y[J, I] greater than 0
                Compute dx = x[J + 1, I] – 1, dy = y[J + 1, I], d = dx^2 + dy^2 }
                    If d < z[J, I]
                        z[J, I] = d, x[J, I] = dx, y[J, I] = dy
    Decrement J and, if J >= 1, repeat
Increment I and, if I <= N, repeat
```

To complete the transform, a second pass in the opposite direction from right to left and top to bottom is made through the data up. The pseudo code for this second pass, shown below, is similar to the previous code apart from the change of direction.

```
Set row index I = N - 1
    Set column index J = N - 1
        If current position has x[J, I] or y[J, I] greater than 0
            If J < N Compute dx = x[J+1, I] - 1, dy = y[J+1, I], d = dx^2 + dy^2
                If d < z[J, I]
                    z[J, I] = d, x[J, I] = dx, y[J, I] = dy
            if I < N Compute dx = x[J, I+1], dy = y[J, I+1] - 1, d = dx^2 + dy^2
                If d < z[J, I]
                    z[J, I] = d, x[J, I] = dx, y[J, I] = dy
    Decrement J and, if J >= 1, repeat
    Set column index J = 1
        If current position has x[J, I] or y[J, I] greater than 0
            Compute dx = x[J - 1, I] + 1, dy = y[J - 1, I], d = dx^2 + dy^2
                If d < z[J, I]
                    z[J, I] = d, x[J, I] = dx, y[J, I] = dy
    Increment J and, if J <= N, repeat
Decrement I and, if I >= 1, repeat
```

On completion of the second pass, the horizontal and vertical offsets of each pixel in the neutral region from the nearest object have been computed. These offsets are used together with the segmented array to identify the polarities of the nearest objects, which then replace the neutral pixel values with the appropriate polarity labels. The resulting boundaries between the positive and negative labelled regions (forming a Voronoi tessellation) indicate the estimated positions of the neutral lines. The neutral lines are marked explicitly by applying a morphological edge detector, to the segmented array.

3 Discussion

The general affect that the value of threshold T has on the resulting neutral lines is illustrated by the sequence of images shown in Fig. 1. From left to right along the top row and then from left to right along the bottom row, the threshold varies in steps of 10 G from 20 to 90 G. The result is a reduction in the number of regions and a simpli-

fication of the boundaries of the resulting regions except where the neutral line separates two regions of strong magnetic field. These latter sections of neutral lines can be identified within the images with larger threshold values as regions where the neutral line possesses fine structure. For comparison, a similar sequence of magnetograms, but with increasing amounts of Gaussian smoothing, is shown in Fig. 2. No attempt has been made to make the smoothing applied to the individual magnetograms in Fig. 2 correspond to the reduction in detail obtained by increasing the threshold value applied to the magnetograms in Fig. 1. Nevertheless, over the central two thirds of the solar magnetograms, in the low field regions, the reduction of detail as the smoothing or threshold value is increased produces similar results. Near the limb, the results are distorted by foreshortening and by boundary effects. Durrant's method [14] reduces this effect by mapping the observed magnetograms to a latitude-longitude grid, applying smoothing and then mapping the result back to the solar disk and this approach could be applied with the distance transform too.

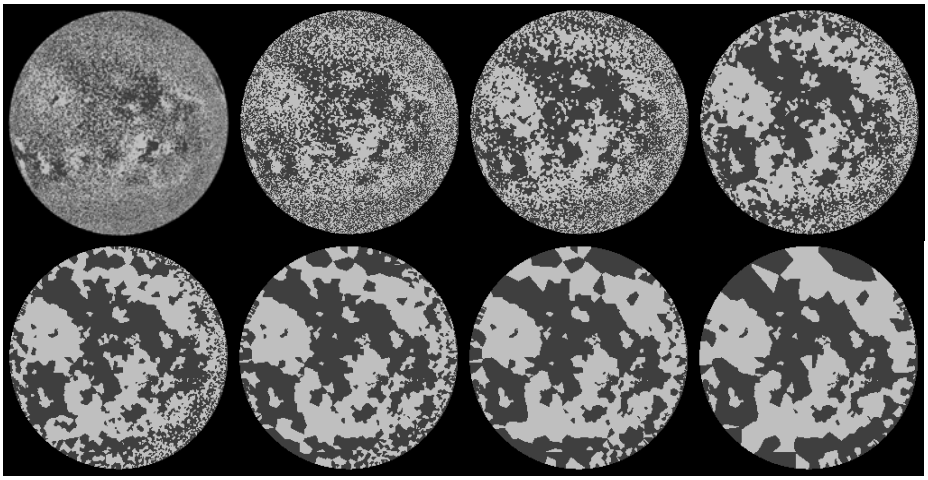

Fig. 1. Magnetic neutral lines indicated by the boundary between dark (negative) and light (positive) regions for thresholds varying from 20 G to 90 G from top left bottom right. MDI July 23 2002.

Examples of magnetic neutral lines, constructed using the distance transform method and using Gaussian smoothing, superimposed on an H-alpha image which has been rescaled and registered to the size and position of the solar disc in the original magnetogram are shown in Fig. 3. It is evident from this figure that in both cases there is a strong correlation between the locations of most of the filaments and inversion lines. The biggest discrepancy is for the large and prominent filament near the top of the image. It lies in a region of positive magnetic polarity and only for lower smoothing/threshold values do its foot points appear close to neutral lines.

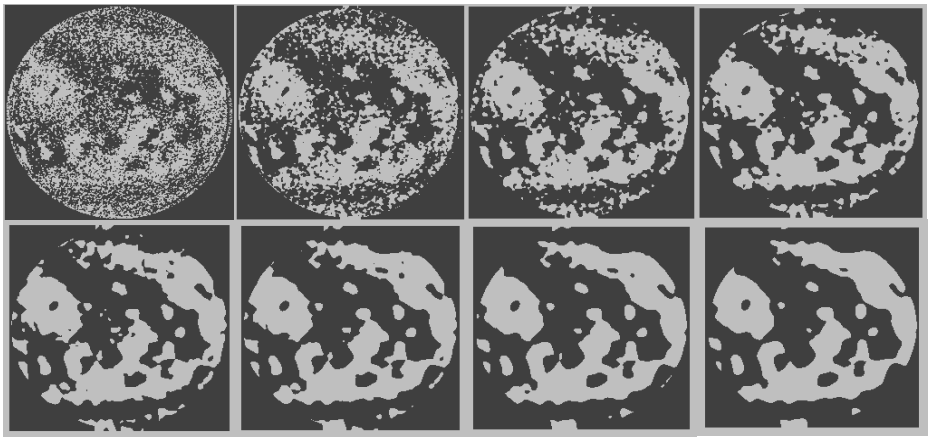

Fig. 2 Neutral lines indicated by the boundary between dark (negative) and light (positive) regions for smoothing radii varying from 5 to 40 from top left bottom right. MDI July 23 2002. In each case the full width of the Gaussian kernel corresponds to 5 standard deviations.

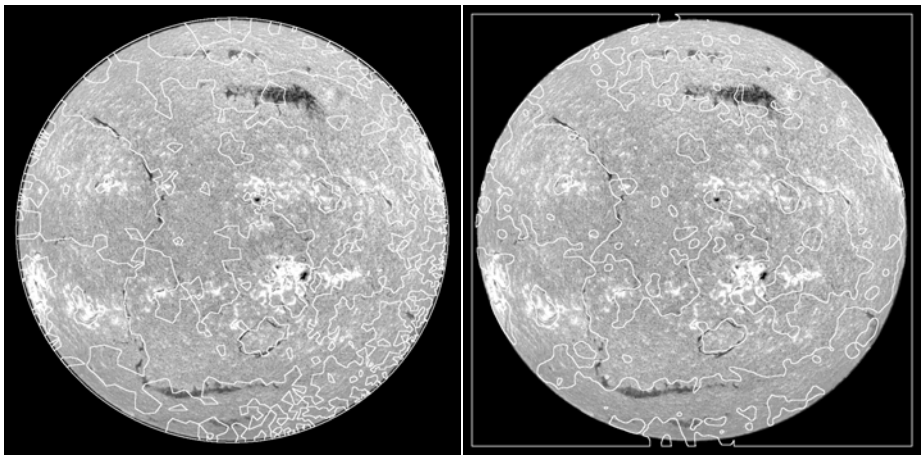

Fig. 3 The composite images show magnetic neutral lines superimposed on an H-alpha image (July 23 2002) from the Meudon observatory. The left hand composite image shows magnetic neutral lines using T = 70 G superimposed on the original magnetogram while the composite image on the right shows magnetic neutral lines using a Gaussian smoothing with a radius of 20 pixel.

4. Conclusions

Two quite different methods of estimating the positions of magnetic neutral lines have been compared. The results found are similar although as the magnetograms are

simplified, in one case by increasing smoothing and in the other by increasing threshold, the distance transform method retains the fine structure in the strong magnetic field regions. In the cases examined most of the filaments are found to be close to neutral lines as suggested in previous literature. This research has been done for the European Grid of Solar Observations (EGSO) funded by the European Commission within the IST Fifth Framework, grant IST-2001-32409.

References

[1] E. R. Priest, "Solar magneto-hydrodynamics", *Geophysics and Astrophysical Monographs*, Dordrecht: Reidel, 1984.

[2] E. Priest and T. Forbes, "Book Rev.: Magnetic reconnection" Cambridge U Press, 2000.

[3] H. V. Babcock and H. D. Babcock, "The Sun's Magnetic Field, 1952-1954", *Astrophysical Journal*, vol. 121, pp.349-366, 1955.

[4] P. H. Scherrer, et al., "Annual Review", *Astr. Astrophys*., Vol. 2, 363, 1995.

[5] H. Wang , C. Denker, T. Spirock, and 7 other authors, "New Digital Magnetograph At Big Bear Solar Observatory" *Solar Physics*, vol. 183, Issue 1, p. 1-13, 1998.

[6] R. K. Ulrich, "In Cool Stars, Stellar Systems and the Sun", edited by M. S. Giampapa and J. A. Bookbinder, *Astron. Soc. of the Pacific, San Francisco*, Calif., p. 265, 1992.

[7] Kippenhahn, and Schluter "Eine Theorie der solaren Filamente", *Zeitschrift für Astrophysik*, vol. 43, p.36-62, 1957.

[8] M. Kuperus and M. A. Raadu, "The Support of Prominences Formed in Neutral Sheets", *Astronomy and Astrophysics*, Vol. 31, pp. 189-193, 1974.

[9] I. Lerche and B. C. Low, "Cylindrical prominences and the magnetic influence of the photospheric boundary2, *Solar Physics*, vol. 66, pp. 285-303, 1980.

[10] B.V. Somov, "Cosmic Plasma Physics", *Astrophysics and Space Science Library*, v. 252. Boston, Mass.:Kluwer Academic Publishing, 2000.

[11] P.A. Sturrock and M. Jardin, "Book Review: Plasma physics" Cambridge U Press, 1994.

[12] D. A. Falconer, R. L. Moore, J. G. Porter, and G. A. Gary, "Neutral-line magnetic shear and enhanced coronal heating in solar active regions", *Astrophysical Journal,* Vol. 482, pp. 519-534, 1997.

[13] P.L. Bornmann, J.R. Winkelman, D. Cook, D. Speich, "Automated solar image processing for flare forecasting", *Solar Terrestrial Workshop*, Hitachi: Japan, pp. 23-27. 1996.

[14] C. J. Durrant, "Polar magnetic fields – filaments and the zero-flux contour", *Solar Phys*., vol. 211, pp. 83-102, 2002.

[15] R. K. Ulrich, S. Evens, J. E. Boyden. and L., Webster, "Mount Wilson synoptic magnetic fields: improved instrumentation, calibration and analysis applied to the 2000 July 14 flare and to the evolution of the dipole field", *Astrophysical Journal Supplement Series*, vol. 139, No. 1, pp. 259-279, 2002.

[16] A. Severny, "Vistas Astron" Vol. 13, p 135, 1972.

[17] R. F. Howard, "Annual Review", *Astron. Astrophys*. Vol. 15, p 153, 1977.

[18] C. Zwaan, "Annual Review", *Astron. Astrophys*. Vol. 25, p 89, 1987.

[19] O. Cuisenaire and B. Macq, "Fast and exact signed Euclidean distance transformation with linear complexity", *In Proc. IEEE Int. Conference on Acoustics, Speech and Signal Processing (ICCASSP99)*, vol. 6, pp. 3293-3296, Phoenix (AZ), March 1999.